

# InfinityHuman: Towards Long-Term Audio-Driven Human Animation

Xiaodi Li<sup>\*1</sup>, Pan Xie<sup>\*1</sup>, Yi Ren<sup>\*2</sup>, Qijun Gan<sup>\*1,2</sup>, Chen Zhang<sup>2</sup>, Fangyuan Kong<sup>1</sup>,  
Xiang Yin<sup>1†</sup>, Bingyue Peng<sup>1</sup>, Zehuan Yuan<sup>1</sup>

<sup>1</sup>ByteDance <sup>2</sup>Zhejiang University

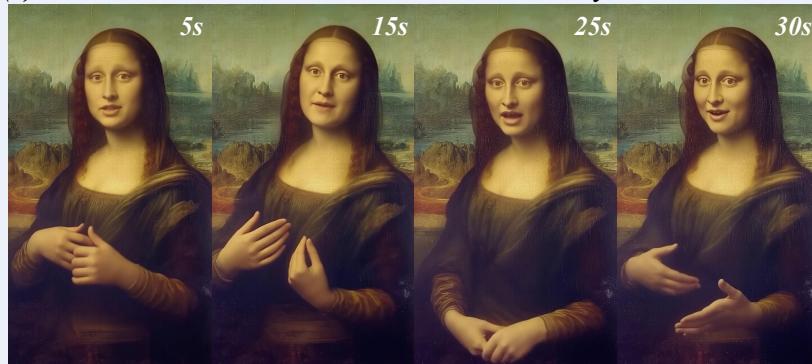
<sup>\*</sup>Equal Contribution <sup>†</sup>Corresponding Author

Project Page: <https://infinityhuman.github.io/>

(a) *long-term id consistency*



(b) *hand motion naturalness & diverse character styles*



(c) *human object interaction*



(d) *emotion control*

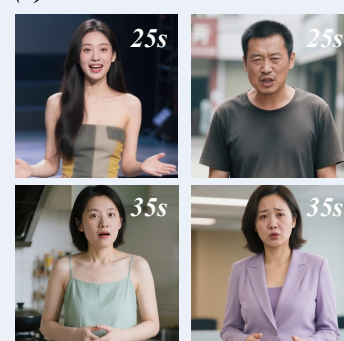


Figure 1: **InfinityHuman** is an audio-driven full-body animation framework that synthesizes long-duration videos with (a) temporally consistent visual appearance, (b) expressive and style-rich hand gestures, (c) dynamic human-object interactions, and (d) emotion-controllable, audio-aligned full-body motions.

## Abstract

Audio-driven human animation has attracted wide attention thanks to its practical applications. However, critical challenges remain in generating high-resolution, long-duration videos with consistent appearance and natural hand motions. Existing methods extend videos using overlapping motion frames but suffer from error accumulation, leading to identity drift, color shifts, and scene instability. Additionally, hand movements are poorly modeled, resulting in noticeable distortions and misalignment with the audio. In this work, we propose InfinityHuman, a coarse-to-fine framework that first generates audio-synchronized representations, then progressively

refines them into high-resolution, long-duration videos using a pose-guided refiner. Since pose sequences are decoupled from appearance and resist temporal degradation, our pose-guided refiner employs stable poses and the initial frame as a visual anchor to reduce drift and improve lip synchronization. Moreover, to enhance semantic accuracy and gesture realism, we introduce a hand-specific reward mechanism trained with high-quality hand motion data. Experiments on the EMTD and HDTF datasets show that InfinityHuman achieves state-of-the-art performance in video quality, identity preservation, hand accuracy, and lip-sync. Ablation studies further confirm the effectiveness of each module. Code will be made public.

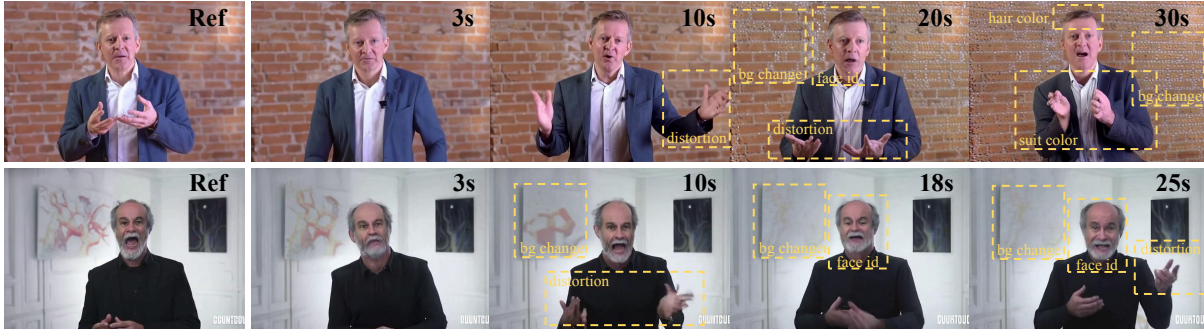


Figure 2: **Progressive Degradation in Long Video Animation by Previous Methods.** Existing methods suffer from cumulative errors leading to pronounced identity drift (facial inconsistencies), color shifts (hair, clothing), scene instability (background fluctuations), and hand motion artifacts. These challenges underscore the necessity of InfinityHuman’s pose-guided refiner and hand-specific optimization for producing high-fidelity, temporally coherent animations over extended sequences.

## 1 Introduction

Audio-driven character animation aims to generate realistic human videos from a single image and audio input, transforming static portraits into speaking characters. This technology holds significant potential across various industries, including advertising, vlogging, and film production. With the rapid advancement of video generation models, recent research (Zhang et al. 2023; Wang et al. 2024a; Lin et al. 2024; Hogue et al. 2024; Cui et al. 2024b; Lin et al. 2025; Wang et al. 2025) has progressed from driving facial and head movements to full-body animation, greatly enhancing the expressiveness and richness of generated content.

Despite notable progress in full-body human animation, critical challenges remain in generating high-resolution, long-duration, and naturally coherent videos. These challenges can be grouped into two main areas: **i) Long-Term Visual Consistency:** Existing methods (Lin et al. 2025; Wang et al. 2025; Chen et al. 2025b; Cui et al. 2024b; Kong et al. 2025; Gan et al. 2025b) typically extend video sequences using overlapping motion frames. However, as sequence length increases, accumulated errors undermine visual coherence, resulting in progressive degradation. This degradation manifests in three key aspects: inconsistent character identity (e.g., variations in facial proportions or clothing); global color incoherence (e.g., erratic shifts in tone or brightness); and scene instability (e.g., shifting or disappearing background objects). **ii) Hand Motion Naturalness:** Prior work has predominantly focused on facial naturalness and coarse body movements, neglecting the nuanced handling of hand motions—small-range yet high-speed movements. Consequently, large hand gestures frequently lead to distortions or artifacts, and misalignment between hand movements and audio further diminishes the expressiveness and realism of generated videos.

To address the aforementioned limitations, we propose **InfinityHuman**, a novel coarse-to-fine generation framework. This framework first produces low-resolution motion frames synchronized with audio, and subsequently outputs high-resolution long-form videos via a dedicated Refiner.

Our method introduces innovations in two key aspects. First, we design a **pose-guided refiner** to address visual drift in long-duration sequences. Given that pose sequences are structurally decoupled from visual appearance, they in-

herently resist temporal degradation in appearance-related features. Consequently, we use them as reliable conditioning signals. In addition, during continuous continuation, we incorporate the initial frame as a visual anchor to further enhance temporal consistency. This combination offers both dynamic guidance for maintaining temporal coherence and a reference for visual fidelity. Furthermore, compared vanilla diffusion-based super-resolution, the pose signal provides strong anatomical structure and preserves fine-grained motion patterns. This enables more accurate lip-syncing while effectively reducing common artifacts such as motion distortions and finger overlap in diffusion-based super-resolution.

Secondly, considering that the human visual system is highly sensitive to hand distortions such as incorrect finger count, unnatural joint movements, we adopt a **hand-specific reward feedback mechanism** and incorporate high-quality hand motion data during training to guide hand generation. The mechanism encourages the model to produce temporally consistent and correct gestures, thereby enhancing character expressiveness and the realism of the video.

We evaluate InfinityHuman on the EMTD (Meng et al. 2024) and HDTF (Zhang et al. 2021) datasets, covering long-duration upper-body and talking-head scenarios. Qualitative and quantitative results show it achieves SOTA performance in video quality, id preservation, hand accuracy, and lip-sync. Ablation studies further confirm the effectiveness of our proposed model. Our contributions are summarized as follows:

- We propose InfinityHuman, a coarse-to-fine generation framework specifically designed to address the challenges of visual realism and temporal consistency in long-duration audio-driven character animation.
- We develop a pose-guided refiner that leverages stable pose sequences and the initial frame as a visual anchor to correct accumulated errors, maintain lip-sync accuracy, and reduce artifacts in extended video sequences.
- To improve hand movement realism and expressiveness, we introduce a hand-specific reward feedback mechanism, integrated with high-quality hand motion data.
- Comprehensive experiments on EMTD and HDTF datasets demonstrate that InfinityHuman outperforms state-of-the-art methods across multiple metrics.

## 2 Related work

**Long Video Generation** Existing methods (Henschel et al. 2024; Bao et al. 2024; Wang et al. 2023; Chen et al. 2024) extend video diffusion models to longer durations by modifying objectives or architectures. Autoregressive pipelines and memory modules (Henschel et al. 2024; Bao et al. 2024) improve cross-segment consistency but require costly retraining on curated long-video datasets. In contrast, training-free extensions such as Gen-L-Video (Wang et al. 2023) and FreeNoise (Qiu et al. 2023) improve efficiency via sliding-window attention and noise rescheduling. However, they offer limited temporal modeling, often causing temporal drift and less coherent transitions between segments. To balance quality and efficiency, recent works (Yin et al. 2025; Zhang and Agrawala 2025; ai et al. 2025) fine-tune short-video diffusion models with previous motion frames as conditions for autoregressive continuation. Despite their flexibility, these methods suffer from error accumulation at inference, leading to degraded fidelity and identity shifts. We adopt a similar strategy but address its limitations with a coarse-to-fine two-stage framework. A low-resolution long video is first generated, followed by a pose-guided refiner that corrects artifacts and restores spatial-temporal consistency, yielding high-resolution, identity-consistent long videos.

**Audio-driven character animation.** Recent advancements in audio-driven character animation have significantly improved lip-syncing and facial expression modulation using latent diffusion models. Works such as SadTalker (Zhang et al. 2023) and Hallo (Xu et al. 2024) enhance audio-to-facial synchronization with 3D rendering and diffusion techniques, while V-Express (Wang et al. 2024a) and EchoMimic (Meng et al. 2024) refine naturalness by integrating audio with facial landmarks and control signals. Loopy (Jiang et al. 2024) and OmniHuman-1 (Lin et al. 2025) ensure identity consistency and mitigate data scarcity through multimodal training. Recent works have extended to full-body animation, with DiffTED (Hogue et al. 2024) introducing a one-shot framework for synchronized talking head and gesture animations, and CyberHost (Lin et al. 2024) enhancing video quality using identity-independent features and human priors. Despite these advancements, generating high-resolution, long-duration, and natural videos remains a significant challenge, particularly in maintaining long-term identity consistency and ensuring the naturalness of hand motions. However, our Infinity Human leverages a pose-guided refiner and hand correction strategies to address these issues.

## 3 Methodology

**Overview.** As shown in Figure 3, InfinityHuman is a unified framework designed to generate long-duration, full-body talking high-resolution videos  $V_{hr}$  from a single reference image  $I_{ref}$ , audio  $c_{audio}$ , and an optional text prompt ( $c_{text}$ ), ensuring visual consistency, precise lip-sync, and natural hand movements. The framework adopts a coarse-to-fine strategy, starting with **Low-Resolution Audio-to-Video**(§3.1) to produce coarse motion in  $V_{lr}$ , followed by **Pose-Guided Refiner**(§3.2) to generate high-resolution video  $V_{hr}$  conditioned on  $V_{lr}$  and  $I_{ref}$ . Additionally, **Hand Correction Strategies**(§3.3) are in-

troduced to enhance the realism and structural integrity of hand movements.

### 3.1 Low-Resolution Audio-to-Video

**Training Objective.** We adopt Flow Matching (Lipman et al. 2022) to train the low-resolution audio-to-video generation (LR-A2V). This approach enables efficient simulation of continuous-time dynamics by learning to predict the data’s velocity field. The backbone of our method is a DiT (Peebles and Xie 2023), denoted as  $f_{\theta}$ , which takes a noisy latent representation as input for all frames  $z^{lr}$ , along with conditioning information from multiple modalities: a reference image  $I_{ref}$ , text condition  $c_{text}$ , audio condition  $c_{audio}$ , and a continuous time step  $t \in [0, 1]$ . The low-resolution latent video  $z^{lr} = \{z_i^{lr}\}_{i=0}^f \in \mathbb{R}^{(f+1) \times h \times w \times c}$  is produced by encoding the input video  $V_{lr}$  using a 3D VAE encoder.

To construct training samples, Gaussian noise  $\epsilon_i \sim \mathcal{N}(0, I)$  is sampled independently for each latent, and the noisy latent at diffusion time  $t$  for latent  $i$  is obtained by the diffusion process:

$$z_{i,t}^{lr} = \phi(z_i^{lr}, t) = (1 - t) \cdot \epsilon_i + t \cdot z_{i,1}^{lr} \quad (1)$$

The target velocity is then defined as:

$$v_{i,t} = \frac{dz_{i,t}^{lr}}{dt} = z_{i,1}^{lr} - \epsilon_i \quad (2)$$

The DiT model is trained to predict these velocities for all frames jointly. The training objective minimizes the expected squared error:

$$\mathcal{L} = \mathbb{E}_{\epsilon_i \sim \mathcal{N}(0, I), t \sim \mathcal{U}(0, 1)} \left\| f_{\theta}(\{z_{i,t}^{lr}\}_{i=0}^f, I_{ref}, c_{text}, c_{audio}, t) - \{v_{i,t}\}_{i=0}^f \right\|_2^2 \quad (3)$$

**Multimodal Condition Attention.** To improve the incorporation and alignment of audio information, we decouple the audio condition from other modalities by introducing a separate cross-attention branch specifically for audio. Formally, the identity-aware cross-attention is extended as follows:

$$CA_{mm}(x^{lr}, c_{text}, c_{audio}) = CA(x^{lr}, c_{text}) + CA(x^{lr}, c_{audio}) \quad (4)$$

In this way, we enable more precise control over multimodal interactions, allowing the model to better align audio cues with visual dynamics and enhance the generation quality.

### 3.2 Pose-Guided Refiner

In long-term generation tasks, low-resolution video  $V_{lr}$  tends to accumulate errors over time, resulting in visual drift where the appearance deviates from the reference image  $I_{ref}$ . To address this issue, the Pose-Guided Refiner (PG-Refiner) leverages the reference image  $I_{ref}$  as an identity prior and conditions on the low-resolution video  $V_{lr}$  along with its corresponding pose sequence  $\mathcal{P} = \{p_i\}_{i=0}^{4f+1}$ . This ensures both temporal coherence in motion and consistent appearance throughout the whole video.

**Low-Resolution Video Latent Condition.** To simulate the temporal degradation phenomenon, we filter out high-frequency signals from the low-resolution latent representation ( $z^{lr}$ ) using a low-pass filter (LPF), and introduce noise



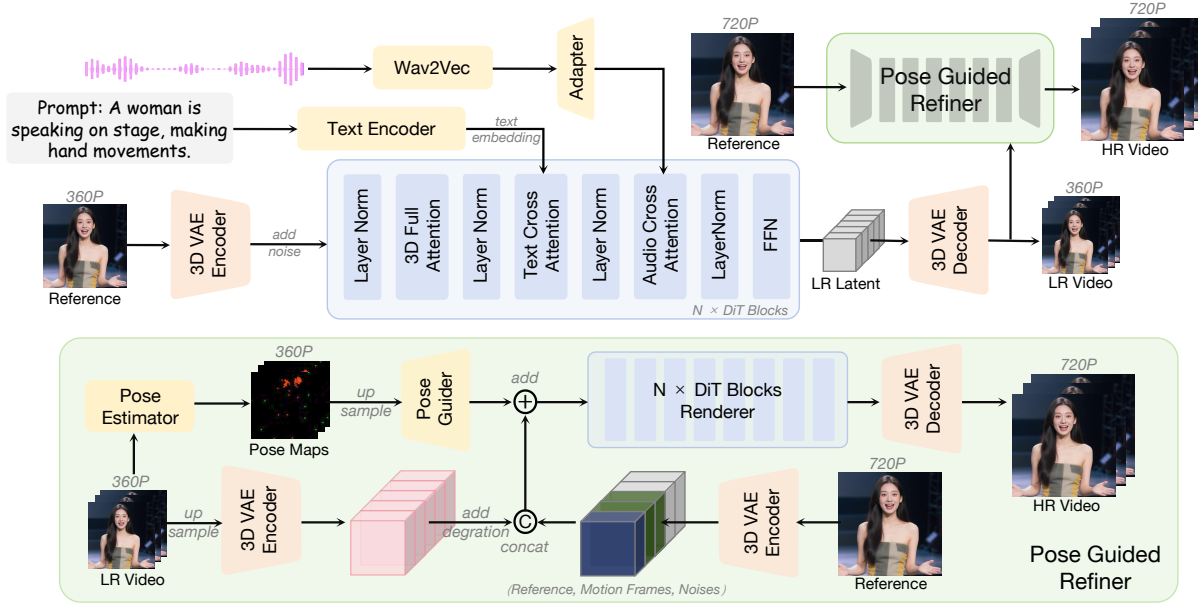


Figure 3: **InfinityHuman Pipeline.** The pipeline generates high-resolution (HR) audio-driven full-body videos through a two-stage coarse-to-fine process. First, a speech-aligned low-resolution (LR) video is generated using multimodal conditioning (text and audio) and DiT blocks. In the second stage, a pose-guided refiner utilizes pose guidance, LR latents, and reference images to restore degraded details, enhancing identity consistency, motion coherence, and hand realism.

augmentation to improve the model’s ability to recover details and correct structural errors. Specifically, the degraded latent representation  $z^{\text{deglr}}$  is computed as:

$$z^{\text{deglr}} = \text{LPF}(z^{\text{lr}}) + \alpha_{\text{deg}} \cdot \epsilon \quad (5)$$

where  $\text{LPF}(z^{\text{lr}})$  extracts the low-frequency components of the video latent,  $\epsilon \sim \mathcal{N}(0, \sigma^2)$  is additive Gaussian noise, and  $\alpha_{\text{deg}}$  controls the noise strength.

**Pose Guidance Condition.** Considering that pose sequence information possesses strong structural properties, preserves fine-grained motions such as lip movements, and remains highly stable with minimal error accumulation in long-duration generation tasks, we adopt it as the condition.

Based on this, we extract human and background keypoints from  $V_{\text{lr}}$ , forming a pose sequence  $\{p_i\}_{i=0}^{4f+1}$ . To avoid scale mismatch and keypoint overlap across different resolutions, we use an 8-channel pixel-level representation: the first 7 channels encode human keypoints, and the last channel encodes up to 20 background keypoints. The resulting pose tensor is denoted as  $\mathcal{P} \in \mathbb{R}^{(4f+1) \times 4h \times 4w \times 8}$ . Accordingly, we apply patchification along the temporal and spatial dimensions: the temporal axis is divided into  $f+1$  segments, and the spatial dimensions into  $h \times w$  patches, yielding pose tokens  $\mathcal{P}' \in \mathbb{R}^{(f+1) \times h \times w \times (64 \times 8)}$ .

These pose tokens are projected into the latent space via a learned projection and fused with the high-resolution latent feature  $z^{\text{hr}}$ , producing a pose-aware latent representation  $z^{\text{hr}} = z^{\text{hr}} + \text{Proj}(\mathcal{P}')$ . The resulting  $z^{\text{hr}}$  serves as the input to the generator, enhancing both visual fidelity and the temporal consistency of motion in the generated video.

**Refiner.** To further enhance temporal consistency, we utilize the initial reference frame as a visual anchor. The Refiner

module leverages the reference image  $I_{\text{ref}}$ , pose conditional features  $P$ , and the low-resolution degraded latent feature  $z^{\text{deglr}}$  to generate high-resolution video frames. Since the model is enhanced with temporal degradation during training and introduces pose information as a control signal that is more direct and structurally informative than audio, it can effectively maintain long-term identity consistency with the assistance of the reference image.

Unlike previous methods (Zeng et al. 2024; Hu et al. 2023) that rely on structure-aligned reference networks, we adopt a prefix-latent reference strategy to ensure identity consistency and enable high-quality long-sequence continuation. This strategy fully exploits the 3D global attention mechanism in the DiT architecture, allowing the model to directly extract identity features from the prefix latent. Specifically, we denote the high-resolution latent sequence as  $\{z_i^{\text{hr}}\}_{i=0}^f$ , where  $z_0^{\text{hr}} = E(I_{\text{ref}})$  is the prefix latent extracted from the reference image using a pretrained 3D VAE encoder  $E(\cdot)$ , and  $z_1^{\text{hr}}$  to  $z_m^{\text{hr}}$  represent motion latents from preceding segments. As the first frame is not temporally compressed,  $z_0^{\text{hr}}$  preserves more detailed information crucial for identity preservation.

During forward diffusion, we inject noise  $\epsilon_i \sim \mathcal{N}(0, I)$  only into the future latents:

$$z_{i,t}^{\text{hr}} = \begin{cases} z_i^{\text{hr}}, & 0 \leq i \leq m, \\ (1-t) \cdot \epsilon_i + t \cdot z_i^{\text{hr}}, & m < i \leq f \end{cases} \quad (6)$$

so that frames 0 through  $m$  remain noise-free to provide stable identity and motion guidance, and their noise predictions are excluded from the loss to maintain reference stability and preserve identity consistency.

Formally, the training objective minimizes the velocity

Method		Video Quality				Lip Sync		ID	Hand Stability	
		FID↓	FVD↓	IQA↑	ASE↑	SYNCS↑	SYND↓	FSIM↑	HKC↑	HKV
HTDF	SadTalker* (Zhang et al. 2023)	147.73	862.83	1.72	1.07	<b>8.87</b>	<b>6.71</b>	<b>0.93</b>	-	-
	AniPortrait* (Wei, Yang, and Wang 2024)	96.12	645.72	1.96	1.15	7.64	7.79	0.85	-	-
	V-Express* (Wang et al. 2024b)	119.45	748.57	1.32	1.16	7.92	7.96	0.89	-	-
	EchoMimic* (Chen et al. 2025c)	167.17	757.38	1.61	1.19	6.71	8.23	0.82	-	-
	HyAva (Chen et al. 2025b)	100.10	662.61	1.52	1.06	7.22	8.98	0.85	-	-
	Hallo3 (Cui et al. 2024b)	74.10	250.12	1.95	1.14	7.31	9.30	0.91	-	-
	MultiTalk (Kong et al. 2025)	85.01	404.45	1.78	1.13	8.76	7.69	0.84	-	-
	OmniAvatar (Gan et al. 2025b)	131.69	705.14	1.67	1.10	8.81	7.76	0.78	-	-
Ours		<b>69.28</b>	<b>239.05</b>	<b>2.11</b>	<b>1.22</b>	8.59	7.53	0.89	-	-
EMTD	Fantasy (Wang et al. 2025)	133.73	1307.20	2.11	1.12	1.11	12.88	0.59	0.57	8.0
	HyAva (Chen et al. 2025b)	139.39	2160.92	1.76	1.18	4.89	9.37	0.67	0.75	29.2
	Hallo3 (Cui et al. 2024b)	104.51	1256.10	2.31	1.48	4.26	10.22	0.73	0.77	6.3
	MultiTalk (Kong et al. 2025)	103.68	1040.43	2.07	1.30	6.34	8.47	0.71	0.79	14.6
	OmniAvatar (Gan et al. 2025b)	82.54	1104.99	2.16	1.31	5.40	9.13	0.72	0.86	28.7
	Ours	<b>60.71</b>	<b>979.88</b>	<b>2.48</b>	<b>1.59</b>	<b>6.56</b>	<b>7.97</b>	<b>0.84</b>	<b>0.90</b>	16.0

Table 1: **Quantitative Comparison of Audio-Driven Animation Methods on EMTD and HTDF.** \* denotes methods limited to talking-head animation. InfinityHuman achieves SOTA results across benchmarks.(§4.2)

prediction error over the noised subset:

$$\mathcal{L}_{\text{ref}} = \mathbb{E}_{\epsilon_i \sim \mathcal{N}(0, I), t \sim \mathcal{U}(0, 1)} \mathbf{w} \cdot \left\| f_{\theta}(\{\mathbf{z}_{i,t}^{\text{hr}}\}_{i=0}^f, \mathbf{z}^{\text{deglr}}, P', I_{\text{ref}}, t) - \{\mathbf{z}_{i,1}^{\text{hr}} - \epsilon_i\}_{i=0}^f \right\|_2^2 \quad (7)$$

where  $\mathbf{w} = \{w_i\}_{i=0}^f$  is a mask vector defined as

$$w_i = \begin{cases} 1, & i > m, \\ 0, & \text{otherwise} \end{cases} \quad (8)$$

To achieve the continuity of motion in long video generation during inference, we take the first  $m$  latents of a new chunk from the last  $m$  latents of the previous chunk, ensuring smooth motion transitions between chunks.

### 3.3 Hand-Specific Reward Feedback Learning

Previous models primarily focus on body and facial movements but overlook detailed hand modeling, leading to unnatural hand distortions in generated videos. To address this, we introduce a hand-specific correction strategy that explicitly targets these artifacts.

The human visual system is highly sensitive to hand structures, with clear perceptual boundaries for distortions such as incorrect finger count, unnatural articulation, or broken textures. Motivated by this, we introduce a preference fine-tuning strategy that directly targets hand realism. By optimizing the diffusion model using reward scores from a pretrained image-level evaluator, we significantly improve the structural fidelity and visual quality of generated hands.

Specifically, we first manually constructed a dataset of 10,000 paired image data of hand structures. Leveraging this carefully domain-specific curated dataset, we performed fine-tuning on the open-source MPS (Zhang et al. 2024) model to enhance its initial capability in capturing hand structural characteristics. Building on this, we leverage the pretrained image-level reward model to assess hand realism. To adapt it for video, we decode the low-resolution latent sequence

$\{z_{m,1}^{\text{lr}}\}_{m=0}^f$  into RGB frames and randomly select one frame  $X_i^{\text{lr}}$  for evaluation. The training objective becomes:

$$\mathcal{L}_{\text{hand}}(\theta) = \mathbb{E}_{c \sim p(c)} \mathbb{E}_{X_i^{\text{lr}} \sim \mathcal{D}(z_{i,1}^{\text{lr}})} [T - r_{\text{hand}}(X_i^{\text{lr}}, c)] \quad (9)$$

where  $X_i^{\text{lr}}$  is a decoded frame randomly sampled from the low-resolution latent trajectory,  $r_{\text{hand}}(\cdot)$  denotes the pre-trained reward model’s assessment of hand quality, and  $T$  denotes the threshold for hand quality. This approach introduces fine-grained, hand-specific supervision without additional annotations, effectively enhancing anatomical plausibility and reducing common distortions in generated human videos.

## 4 Experiment

### 4.1 Implementation Details

**Datasets.** Our data processing pipeline is as follows: First, we employ SceneDetect (Brandon 2024) for temporal cropping of the raw videos. Next, we use YOLO (Jocher, Qiu, and Chaurasia 2023) to track the single person, obtain corresponding spatiotemporal bounding boxes, and perform spatiotemporal cropping. Additionally, videos are filtered based on criteria including video quality, aesthetics, motion amplitude, hand clarity, mouth clarity, and the proportion of the person within the frame. Ultimately, this process yields 7,700 hours of single-person video clips, which is used to train the pose-guider refiner. Building on this dataset, SyncNet (Chung and Zisserman 2017) is further employed to assess the synchronization between audio and mouth movements, filtering to obtain 1,800 hours of clips for training low-resolution audio-driven video generation, where each clip is 4 seconds. **Training.** To train audio-driven low-resolution video generation, we begin with a pretrained Goku-I2V (Chen et al. 2025a) model. For video generation training conditioned on multiple modalities, we include reference images, first frames, audio, and text as modal conditions. A multiple conditions dropout strategy is applied during training to enhance robustness. Specifically, text and audio are dropped with a 10% probability independently. Meanwhile, the reference image and first frame are each dropped with a 20% probability.

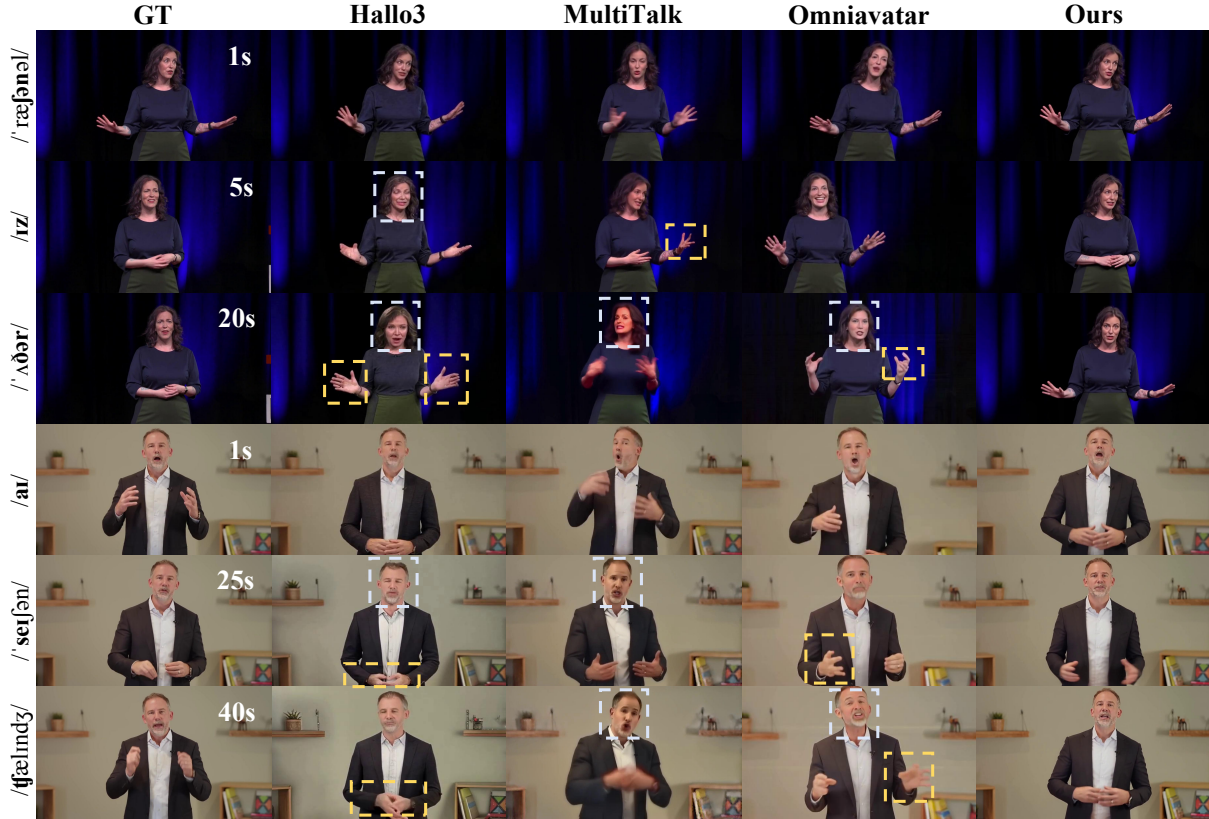


Figure 4: **Qualitative Results of Audio-Driven Animation Methods on EMTD.** Yellow and blue boxes highlight hand distortions and face ID mismatches, respectively. The results demonstrate the superiority of InfinityHuman in maintaining identity consistency, lip-sync accuracy, and visual fidelity during long-duration generation. Please zoom in for details. (§4.2)

To train pose-guided refiner, we also use Goku-I2V as pre-trained base model. We adopt the training strategy from Humandit (Gan et al. 2025a), exposing the model to a range of resolutions to enable effective learning across diverse video qualities and sizes. Our conditioning modalities include pose extracted via Sapines (Khirodkar et al. 2024), first-frame reference images, and low-resolution 3D VAE latents. During training, a dropout mechanism is applied: both pose and low-resolution latents are dropped with a 20% probability.

Both two models are trained using 128 NVIDIA GPUs with a learning rate of  $5e-5$ . For LR-A2V inference, we apply audio and text classifier-free guidance (CFG) (Ho and Salimans 2022) set to 6.5 and 30 denoising steps. For PG-Refiner, we apply pose CFG set to 1.5 and 20 denoising steps. Furthermore, we distill the PG-Refiner into a 1-step model while preserving output quality, enabling ultra-fast low-resolution generation and efficient high-resolution refinement with minimal steps. Detailed inference speed comparisons are provided in the appendix.

## 4.2 Comparison with State-of-the-Art Methods

**Evaluation Metrics.** To evaluate our model, we use a comprehensive video quality metric combining FID (Heusel et al. 2017) for image quality, FVD (Unterthiner et al. 2018) for video dynamics, and Q-align (Wu et al. 2023) for visual quality (IQA) and aesthetic appeal (AES). Lip-sync accuracy is assessed using Sync-C and Sync-D (Chung and Zisserman 2017), while identity consistency is measured with

FaceSIM (Yuan et al. 2025; Huang et al. 2024). For hand evaluation, we use average Hand Keypoint Confidence (HKC) and Hand Keypoint Variance (HKV).

**Test Datasets & Baselines.** For evaluation, we use the EMTD (Meng et al. 2024) dataset, which contains 110 720P speech videos covering the upper body and hands. The longest video lasts 74 seconds, with 23.64% of the videos exceeding 15 seconds, making it well-suited for assessing audio-driven portrait video generation in high-resolution, long-duration scenarios. To further evaluate the generalization ability of our method, we additionally select 100 samples from the HDTF (Zhang et al. 2021) dataset at a resolution of  $512 \times 512$  as a talking-face test set. We also conduct a user test, detailed in the appendix.

We compare InfinityHuman with human animation methods, including FantasyTalking (Wang et al. 2025), Hallo3 (Cui et al. 2024a), HunyuanAvatar (Chen et al. 2025b), MultiTalk (Kong et al. 2025), and OmniAvatar (Gan et al. 2025b), evaluated on the EMTD dataset. Since OmniHuman (Lin et al. 2025) is limited to 15-second videos and lacks long-form continuation support, it is excluded from the long-video evaluation. For short-video comparison, please refer to the appendix. In addition, we evaluate our method on the talking face generation benchmark HDTF (Zhang et al. 2021), comparing it with methods such as SadTalker (Zhang et al. 2023), Aniportrait (Wei, Yang, and Wang 2024), V-express (Wang et al. 2024b), EchoMimic (Chen et al. 2025c),



Method	FID↓	FVD↓	FSIM↑	HKC↑
w/o refiner	109.54	876.49	0.79	0.85
w/o lr cond	91.92	1001.00	0.86	0.85
w/o pose cond	156.74	1163.75	0.83	0.83
w/o hand refl	86.32	844.57	0.86	0.85
ours	<b>91.74</b>	<b>758.98</b>	<b>0.88</b>	<b>0.87</b>

Table 2: **Quantitative Ablation Study.** Demonstrating the effectiveness of the pose-guided refiner and its corresponding conditions, including low-resolution video latent condition, pose guidance condition (§3.2), and hand-specific refl (§3.3).

and other representative full-body models.

**Qualitative Results & Quantitative Results.** For quantitative comparison, as shown in Table 1, our method achieves the best results in both FID and FVD across the audio-driven head and full-body animation tasks. Specifically, on the EMTD dataset, our model achieves an FID of 60.71 and an FVD of 979.88, outperforming the previous best results of 82.54 (OmniAvatar) and 1040.43 (MultiTalk), respectively. Notably, in full-body animation, our method achieves stronger identity consistency, with a FaceSIM of 0.84 (vs. 0.73 for Hallo3). It also delivers better hand motion quality, reaching the highest HKC of 0.90. These improvements demonstrate that our model generates videos that are both more visually realistic and exhibit better temporal coherence.

Additionally, we conduct a qualitative evaluation, as illustrated in Figure 4. Our method demonstrates the ability to generate highly consistent and visually coherent animations over long sequences, maintaining a strong alignment with the corresponding audio. For instance, in the 40-second case, our approach ensures consistent id preservation and color harmony throughout the video. In contrast, other methods exhibit noticeable discrepancies in skin tone, hair color, and facial shapes, especially during long video continuations.

Our method also excels in hand generation, particularly when handling complex hand movements. While other models often struggle with severe distortions or unnatural gestures, our method ensures stable and realistic hand movements, even in challenging poses like hand crossing. This further underscores the superiority of our approach in managing intricate visual dynamics.

### 4.3 Ablation Study And Discussion

**Ablation on the pose-guided refiner.** By removing the pose-guided refiner, we directly decode videos from the low-resolution generator on a subset of the EMTD dataset to evaluate its effectiveness. As shown in Table 2, the overall generation quality significantly degrades, with FID increasing from 91.74 to 109.54 and FSIM dropping from 0.88 to 0.79. As illustrated in Figure 5, the degradation is particularly evident in blurred facial details and reduced temporal consistency. These results highlight the critical role of the refiner in recovering visual quality, enhancing temporal stability, and preserving identity over long sequences.

Furthermore, given that the refiner relies on multiple conditional inputs with non-trivial interdependencies, we conduct a deeper analysis of their individual contributions and guidance strength. As shown in Figure 5, omitting either the pose



Figure 5: **Visualization of Ablation Study.** Demonstrating the effects of key components on animation quality.

information or low-resolution latent features after training leads to color shifts and structural degradation in long-term video generation. This suggests that both inputs serve as essential references: the pose offers accurate structural constraints, while the low-resolution latent helps preserve overall semantic content and stylistic consistency.

**Ablation on the hand-specific reward feedback learning.** We also assess the impact of the hand-specific reward feedback (refl) mechanism on generation performance. As shown in Table 2, removing it from the full model results in a decline in hand keypoint accuracy, with HKC decreasing from 0.87 to 0.85. Qualitatively, more artifacts and discontinuities appear in the hand regions, especially in sequences involving complex or high-speed gestures. These findings demonstrate that the hand-specific reward plays a vital role in improving the realism, stability, and audio synchronization of hand motion, particularly under challenging gestural conditions.

## 5 Conclusion and Future Work

We present InfinityHuman, a coarse-to-fine framework for high-fidelity, long-duration, audio-driven full-body human animation. By introducing a pose-guided refiner and a hand-specific reward mechanism, our approach effectively addresses key challenges in visual consistency, lip-sync accuracy, and hand motion realism. Extensive experiments on EMTD and HDTF demonstrate that InfinityHuman achieves state-of-the-art performance across multiple metrics.

A limitation of our current framework is that it is trained solely on continuous single-person footage, which restricts its ability to handle multi-person interactions and complex scene transitions such as shot changes or cuts. Extending InfinityHuman to support multi-person generation and dynamic scene transitions is an important direction for future work.

## References

- ai, S.; Teng, H.; Jia, H.; Sun, L.; Li, L.; Li, M.; Tang, M.; Han, S.; Zhang, T.; Zhang, W. Q.; Luo, W.; Kang, X.; Sun, Y.; Cao, Y.; Huang, Y.; Lin, Y.; Fang, Y.; Tao, Z.; Zhang, Z.; Wang, Z.; Liu, Z.; Shi, D.; Su, G.; Sun, H.; Pan, H.; Wang, J.; Sheng, J.; Cui, M.; Hu, M.; Yan, M.; Yin, S.; Zhang, S.; Liu, T.; Yin, X.; Yang, X.; Song, X.; Hu, X.; Zhang, Y.; and Li, Y. 2025. MAGI-1: Autoregressive Video Generation at Scale. *arXiv:2505.13211*.
- Bao, F.; Xiang, C.; Yue, G.; He, G.; Zhu, H.; Zheng, K.; Zhao, M.; Liu, S.; Wang, Y.; and Zhu, J. 2024. Vidu: a Highly Consistent, Dynamic and Skilled Text-to-Video Generator with Diffusion Models. *arXiv preprint arXiv:2405.04233*.
- Brandon, C. 2024. PySceneDetect. <https://github.com/Breakthrough/PySceneDetect/>.
- Chen, S.; Ge, C.; Zhang, Y.; Zhang, Y.; Zhu, F.; Yang, H.; Hao, H.; Wu, H.; Lai, Z.; Hu, Y.; et al. 2025a. Goku: Flow based video generative foundation models. In *Proceedings of the Computer Vision and Pattern Recognition Conference*, 23516–23527.
- Chen, T.-S.; Siarohin, A.; Menapace, W.; Deyneka, E.; Chao, H.-w.; Jeon, B. E.; Fang, Y.; Lee, H.-Y.; Ren, J.; Yang, M.-H.; et al. 2024. Panda-70m: Captioning 70m videos with multiple cross-modality teachers. In *Proceedings of the IEEE/CVF Conference on Computer Vision and Pattern Recognition*, 13320–13331.
- Chen, Y.; Liang, S.; Zhou, Z.; Huang, Z.; Ma, Y.; Tang, J.; Lin, Q.; Zhou, Y.; and Lu, Q. 2025b. HunyuanVideo-Avatar: High-Fidelity Audio-Driven Human Animation for Multiple Characters. *arXiv:2505.20156*.
- Chen, Z.; Cao, J.; Chen, Z.; Li, Y.; and Ma, C. 2025c. Echomimic: Lifelike audio-driven portrait animations through editable landmark conditions. In *Proceedings of the AAAI Conference on Artificial Intelligence*, volume 39, 2403–2410.
- Chung, J. S.; and Zisserman, A. 2017. Out of time: automated lip sync in the wild. In *Computer Vision—ACCV 2016 Workshops: ACCV 2016 International Workshops, Taipei, Taiwan, November 20–24, 2016, Revised Selected Papers, Part II 13*, 251–263. Springer.
- Cui, J.; Li, H.; Zhan, Y.; Shang, H.; Cheng, K.; Ma, Y.; Mu, S.; Zhou, H.; Wang, J.; and Zhu, S. 2024a. Hallo3: Highly Dynamic and Realistic Portrait Image Animation with Diffusion Transformer Networks. *arXiv preprint arXiv:2412.00733*.
- Cui, J.; Li, H.; Zhan, Y.; Shang, H.; Cheng, K.; Ma, Y.; Mu, S.; Zhou, H.; Wang, J.; and Zhu, S. 2024b. Hallo3: Highly Dynamic and Realistic Portrait Image Animation with Video Diffusion Transformer. *arXiv preprint arXiv:2412.00733*.
- Gan, Q.; Ren, Y.; Zhang, C.; Ye, Z.; Xie, P.; Yin, X.; Yuan, Z.; Peng, B.; and Zhu, J. 2025a. Humandit: Pose-guided diffusion transformer for long-form human motion video generation. *arXiv preprint arXiv:2502.04847*.
- Gan, Q.; Yang, R.; Zhu, J.; Xue, S.; and Hoi, S. 2025b. Omni-Avatar: Efficient Audio-Driven Avatar Video Generation with Adaptive Body Animation. *arXiv preprint arXiv:2506.18866*.
- Henschel, R.; Khachatryan, L.; Hayrapetyan, D.; Poghosyan, H.; Tadevosyan, V.; Wang, Z.; Navasardyan, S.; and Shi, H. 2024. StreamingT2V: Consistent, Dynamic, and Extendable Long Video Generation from Text. *arXiv preprint arXiv:2403.14773*.
- Heusel, M.; Ramsauer, H.; Unterthiner, T.; Nessler, B.; and Hochreiter, S. 2017. Gans trained by a two time-scale update rule converge to a local nash equilibrium. *Advances in neural information processing systems*, 30.
- Ho, J.; and Salimans, T. 2022. Classifier-free diffusion guidance. *arXiv preprint arXiv:2207.12598*.
- Hogue, S.; Zhang, C.; Daruger, H.; Tian, Y.; and Guo, X. 2024. DiffTED: One-shot Audio-driven TED Talk Video Generation with Diffusion-based Co-speech Gestures. In *Proceedings of the IEEE/CVF Conference on Computer Vision and Pattern Recognition*, 1922–1931.
- Hu, L.; Gao, X.; Zhang, P.; Sun, K.; Zhang, B.; and Bo, L. 2023. Animate anyone: Consistent and controllable image-to-video synthesis for character animation. *arXiv preprint arXiv:2311.17117*.
- Huang, J.; Dong, X.; Song, W.; Chong, Z.; Tang, Z.; Zhou, J.; Cheng, Y.; Chen, L.; Li, H.; Yan, Y.; et al. 2024. Consistent: Portrait generation with multimodal fine-grained identity preserving. *arXiv preprint arXiv:2404.16771*.
- Jiang, J.; Liang, C.; Yang, J.; Lin, G.; Zhong, T.; and Zheng, Y. 2024. Loopy: Taming Audio-Driven Portrait Avatar with Long-Term Motion Dependency. *arXiv preprint arXiv:2409.02634*.
- Jocher, G.; Qiu, J.; and Chaurasia, A. 2023. Ultralytics YOLO. <https://github.com/ultralytics/ultralytics>.
- Khrodar, R.; Bagautdinov, T.; Martinez, J.; Zhaoen, S.; James, A.; Selednik, P.; Anderson, S.; and Saito, S. 2024. Sapiens: Foundation for Human Vision Models. *arXiv preprint arXiv:2408.12569*.
- Kong, Z.; Gao, F.; Zhang, Y.; Kang, Z.; Wei, X.; Cai, X.; Chen, G.; and Luo, W. 2025. Let Them Talk: Audio-Driven Multi-Person Conversational Video Generation. *arXiv preprint arXiv:2505.22647*.
- Lin, G.; Jiang, J.; Liang, C.; Zhong, T.; Yang, J.; and Zheng, Y. 2024. CyberHost: Taming Audio-driven Avatar Diffusion Model with Region Codebook Attention. *arXiv preprint arXiv:2409.01876*.
- Lin, G.; Jiang, J.; Yang, J.; Zheng, Z.; and Liang, C. 2025. OmniHuman-1: Rethinking the Scaling-Up of One-Stage Conditioned Human Animation Models. *arXiv preprint arXiv:2502.01061*.
- Lipman, Y.; Chen, R. T.; Ben-Hamu, H.; Nickel, M.; and Le, M. 2022. Flow matching for generative modeling. *arXiv preprint arXiv:2210.02747*.
- Meng, R.; Zhang, X.; Li, Y.; and Ma, C. 2024. EchoMimicV2: Towards Striking, Simplified, and Semi-Body Human Animation. *arXiv preprint arXiv:2411.10061*.
- Peebles, W.; and Xie, S. 2023. Scalable diffusion models with transformers. In *Proceedings of the IEEE/CVF international conference on computer vision*, 4195–4205.



- Qiu, H.; Xia, M.; Zhang, Y.; He, Y.; Wang, X.; Shan, Y.; and Liu, Z. 2023. Freenoise: Tuning-free longer video diffusion via noise rescheduling. *arXiv preprint arXiv:2310.15169*.
- Ren, Y.; Xia, X.; Lu, Y.; Zhang, J.; Wu, J.; Xie, P.; Wang, X.; and Xiao, X. 2024. Hyper-sd: Trajectory segmented consistency model for efficient image synthesis. *Advances in Neural Information Processing Systems*, 37: 117340–117362.
- Sauer, A.; Boesel, F.; Dockhorn, T.; Blattmann, A.; Esser, P.; and Rombach, R. 2024. Fast high-resolution image synthesis with latent adversarial diffusion distillation. In *SIGGRAPH Asia 2024 Conference Papers*, 1–11.
- Unterthiner, T.; Van Steenkiste, S.; Kurach, K.; Marinier, R.; Michalski, M.; and Gelly, S. 2018. Towards accurate generative models of video: A new metric & challenges. *arXiv preprint arXiv:1812.01717*.
- Wang, C.; Tian, K.; Zhang, J.; Guan, Y.; Luo, F.; Shen, F.; Jiang, Z.; Gu, Q.; Han, X.; and Yang, W. 2024a. V-Express: Conditional Dropout for Progressive Training of Portrait Video Generation. *arXiv preprint arXiv:2406.02511*.
- Wang, C.; Tian, K.; Zhang, J.; Guan, Y.; Luo, F.; Shen, F.; Jiang, Z.; Gu, Q.; Han, X.; and Yang, W. 2024b. V-express: Conditional dropout for progressive training of portrait video generation. *arXiv preprint arXiv:2406.02511*.
- Wang, F.-Y.; Chen, W.; Song, G.; Ye, H.-J.; Liu, Y.; and Li, H. 2023. Gen-l-video: Multi-text to long video generation via temporal co-denoising. *arXiv preprint arXiv:2305.18264*.
- Wang, F.-Y.; Huang, Z.; Bergman, A.; Shen, D.; Gao, P.; Lingelbach, M.; Sun, K.; Bian, W.; Song, G.; Liu, Y.; et al. 2024c. Phased consistency models. *Advances in neural information processing systems*, 37: 83951–84009.
- Wang, M.; Wang, Q.; Jiang, F.; Fan, Y.; Zhang, Y.; Qi, Y.; Zhao, K.; and Xu, M. 2025. FantasyTalking: Realistic Talking Portrait Generation via Coherent Motion Synthesis. *arXiv preprint arXiv:2504.04842*.
- Wei, H.; Yang, Z.; and Wang, Z. 2024. Aniportrait: Audio-driven synthesis of photorealistic portrait animation. *arXiv preprint arXiv:2403.17694*.
- Wu, H.; Zhang, Z.; Zhang, W.; Chen, C.; Liao, L.; Li, C.; Gao, Y.; Wang, A.; Zhang, E.; Sun, W.; et al. 2023. Q-align: Teaching Imms for visual scoring via discrete text-defined levels. *arXiv preprint arXiv:2312.17090*.
- Xie, L.; Li, Y.; Du, S.; Xia, M.; Wang, X.; Yu, F.; Chen, Z.; Wan, P.; Zhou, J.; and Dong, C. 2025. SimpleGVR: A Simple Baseline for Latent-Cascaded Video Super-Resolution. *arXiv preprint arXiv:2506.19838*.
- Xu, M.; Li, H.; Su, Q.; Shang, H.; Zhang, L.; Liu, C.; Wang, J.; Van Gool, L.; Yao, Y.; and Zhu, S. 2024. Hallo: Hierarchical Audio-Driven Visual Synthesis for Portrait Image Animation. *arXiv preprint arXiv:2406.08801*.
- Yin, T.; Zhang, Q.; Zhang, R.; Freeman, W. T.; Durand, F.; Shechtman, E.; and Huang, X. 2025. From Slow Bidirectional to Fast Autoregressive Video Diffusion Models. In *CVPR*.
- Yuan, S.; Huang, J.; He, X.; Ge, Y.; Shi, Y.; Chen, L.; Luo, J.; and Yuan, L. 2025. Identity-preserving text-to-video generation by frequency decomposition. In *Proceedings of the Computer Vision and Pattern Recognition Conference*, 12978–12988.
- Zeng, Y.; Wei, G.; Zheng, J.; Zou, J.; Wei, Y.; Zhang, Y.; and Li, H. 2024. Make pixels dance: High-dynamic video generation. In *Proceedings of the IEEE/CVF Conference on Computer Vision and Pattern Recognition*, 8850–8860.
- Zhang, L.; and Agrawala, M. 2025. Packing Input Frame Contexts in Next-Frame Prediction Models for Video Generation. *Arxiv*.
- Zhang, S.; Wang, B.; Wu, J.; Li, Y.; Gao, T.; Zhang, D.; and Wang, Z. 2024. Learning multi-dimensional human preference for text-to-image generation. In *Proceedings of the IEEE/CVF Conference on Computer Vision and Pattern Recognition*, 8018–8027.
- Zhang, W.; Cun, X.; Wang, X.; Zhang, Y.; Shen, X.; Guo, Y.; Shan, Y.; and Wang, F. 2023. Sadtalker: Learning realistic 3d motion coefficients for stylized audio-driven single image talking face animation. In *Proceedings of the IEEE/CVF conference on computer vision and pattern recognition*, 8652–8661.
- Zhang, Z.; Li, L.; Ding, Y.; and Fan, C. 2021. Flow-guided one-shot talking face generation with a high-resolution audio-visual dataset. In *Proceedings of the IEEE/CVF conference on computer vision and pattern recognition*, 3661–3670.

## 6 Appendix

In this supplementary material, we provide additional technical details, experiment results, and design considerations that support the main paper. The content is organized as follows:

- Short Baseline Comparisons (Sec. 6.1);
- Detailed Parameters and Training Strategies (Sec. 6.2);
- Multi-person Video Discussion and Solutions (Sec. 6.3);
- Speed Benchmark (Sec. 6.4);
- Hand-Specific Refl Generalization (Sec. 6.5);
- User Study Results (Sec. 6.6);
- Long-Form Video Stability (Sec. 6.7);
- Societal Impacts (Sec. 6.8);
- More Demo Cases (Sec. 6.9);

### 6.1 Short Baseline Comparisons



Figure 6: Qualitative comparison between OmniHuman and our method on 15s clips. Our model preserves finer facial details and produces more stable hand movements.

OmniHuman (Lin et al. 2025) is limited to generating videos up to 15 seconds in length and lacks support for long-form temporal modeling, making it unsuitable for long-video evaluations presented in the main paper. Hence, we provide a dedicated comparison in the short-video setting (under 15 seconds).

Model	FID ↓	FVD ↓	FSIM ↑	HKC ↑	Sync-C ↑
OmniHuman	89.91	723.14	0.81	0.886	8.14
Ours	<b>77.05</b>	<b>540.89</b>	<b>0.88</b>	<b>0.894</b>	<b>8.98</b>

Table 3: Quantitative comparison on short videos (under 15s) with OmniHuman.

As shown in Table 3, our model consistently outperforms OmniHuman across all evaluation metrics on short video generation. While OmniHuman achieves reasonable quality in short segments, our method delivers higher visual fidelity (lower FID and FVD), better structural similarity (FSIM), improved keypoint consistency (HKC), and stronger audio-visual synchronization (Sync-C), indicating enhanced short-term realism and coherence.

Figure 6 provides a qualitative frame-by-frame comparison. OmniHuman occasionally exhibits identity inconsistency and distorted hand shapes, whereas our method generates more temporally consistent gestures and better-preserved facial features throughout the sequence.

### 6.2 Detailed Parameters and Training Strategies

For hand-specific reward model, to construct data pairs for training a "hand distortion" dimension, we follow a methodology inspired by the Multi-dimensional Human Preference (MHP) dataset (Zhang et al. 2024) construction process, with specific adaptations for hand-related evaluation. First, prompt collection focuses on scenarios involving hands to ensure targeted data generation. Next, image generation utilizes several state-of-the-art text-to-image models. Each model generates 2–4 images per prompt, yielding approximately 40,000 images. This diversity ensures coverage of varying hand distortion patterns across model types and settings. For annotation, a crowdsourced team of 10 annotators is trained with clear guidelines: hand distortion is defined as abnormal finger count, twisting, blurriness, structural incoherence (e.g., missing joints), or misalignment with context (e.g., a "grasping" hand without closed fingers). Annotators rate each image in a pair on a 1–5 scale (1 = severe distortion, 5 = perfect integrity) for the "hand distortion" dimension.

For aesthetic evaluation, the T-score threshold was empirically set to 0.4. In addition, our dataset includes multilingual content, enabling the model to support input in various languages and generate corresponding results across different linguistic contexts.

In our Low-Resolution Noise Injection Strategy, Gaussian noise is added to the low-resolution encoder and scaled by a factor  $\alpha$ . We found that  $\alpha = 0.7$  achieves the best trade-off between visual realism and temporal stability. Consistent with observations in SimpleGVR (Xie et al. 2025), we noted that training with small noise levels ( $\alpha \in [0.0, 0.3]$ ) led to suboptimal refinement of fine details. In contrast, using higher

noise levels ( $\alpha \in [0.6, 0.9]$ ) enabled the model to better recover detail structures, especially when guided by pose estimation.

For pose extraction, we employ the Sapiens estimator (Khirrodar et al. 2024), which demonstrates robust performance across a wide range of motion types.

For evaluation, we used different prompts across datasets. The EMTD prompt is: “A realistic video of a man/woman speaking directly to the camera, waving his/her hand with dynamic and rhythmic hand gestures that complement the speech. His/Her hands are clearly visible, independent and unobstructed. Facial expressions are expressive and full of emotion, enhancing the delivery. The camera remains steady, capturing sharp, clear movements and a focused, engaging presence.” For HDTF, we use the same prompt without the hand gesture sentence.

### 6.3 Multi-person Video Discussion and Solutions

Handling multi-person scenarios introduces challenges such as accurate pose assignment, occlusion management, and audio-motion alignment. Since our training data primarily consists of single-person, continuous video clips, directly applying our model to reference images containing multiple individuals and alternating speech audio may result in incorrect behavior—such as both people speaking simultaneously. As shown in Fig. 7, when no control is applied, both characters erroneously respond to the same speech input.

To address this, we propose a simple extension based on fixed bounding boxes and an audio-aware attention mechanism to preliminarily support multi-person video generation. Specifically, for each human bounding box (e.g., bbox1 and bbox2), we introduce directional audio control in the cross-attention module. For the currently speaking character (e.g., bbox1), the visual features are attended to using the actual speech audio features; for the non-speaking character (e.g., bbox2), we input silent audio features to suppress unintended movements. This approach enables synchronized turn-taking behavior between characters without modifying the core network architecture. As shown in Fig. 7, our strategy enables clear alternation of speaking roles between multiple characters.

However, because our model is not trained on multi-person data, it lacks the ability to handle rich interactions such as mutual gaze, coordinated gestures, or conversational feedback. Additionally, the current Pose-Guided Refiner module, which relies on additive conditioning, is not yet capable of processing multiple pose streams simultaneously.

In summary, while our approach provides a lightweight and scalable extension for basic multi-person, alternating-speech scenarios, generating dynamic, interactive multi-character talking videos remains a challenging direction for future research. Progress in dataset construction and model architecture will be crucial to further advance this capability.

### 6.4 Speed Benchmark

We applied distillation acceleration on 720p-Refiner. First, we employed PCM (Wang et al. 2024c; Ren et al. 2024) for step distillation, compressing it to 4 steps inference. Then,

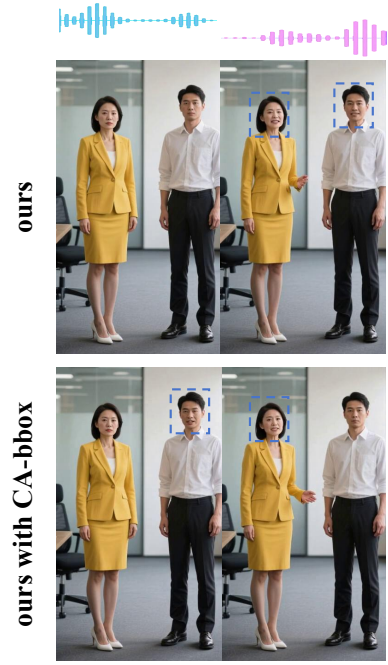


Figure 7: Illustration of multi-person alternating speaking. Without control, both characters speak simultaneously. With audio-aware attention and bounding box assignment, only the target character moves, while the other remains idle.

we used LADD (Sauer et al. 2024) for adversarial training. Finally, we achieve Refiner-distill with one-step inference.

We selected a 720P-resolution subset from our validation set to benchmark the inference efficiency and generation quality of different models. Specifically, we compared our model before and after knowledge distillation, evaluating both runtime and quality metrics.

Table 4 summarizes the inference time and quality metrics (FID and FVD) across models on this subset. Our distilled model significantly reduces inference time while maintaining stable performance compared to the pre-distilled version.

This efficiency gain is attributed to our coarse-to-fine architecture: the majority of denoising steps are performed at a lower resolution (e.g., 360P), with only a few refinement steps conducted at the high-resolution stage. This design effectively reduces computation while preserving final output fidelity, demonstrating the practical advantages of our method in real-time generation scenarios.

Model	Aud. (s)	Inf. Time (s)	FID ↓	FVD ↓
LR-A2V + Refiner	16.4	552	50.51	909.82
LR-A2V + Refiner-distill	16.4	187	48.17	884.27

Table 4: Inference Time and Quality Metrics. Distilled model reduces time while maintaining quality.

As shown in Figure 8, the perceptual quality between the distilled and original versions is nearly indistinguishable. While the distilled model may produce slightly sharper edges and less background blending in some frames, the overall visual fidelity remains high.



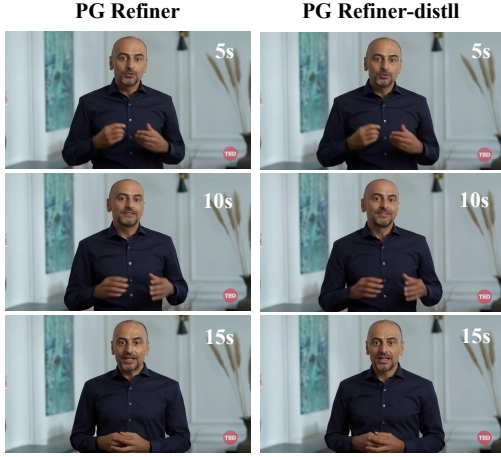


Figure 8: Visual comparison between the original and distilled model outputs. Perceptual difference is minimal, though the distilled version tends to produce slightly sharper foregrounds and less blended backgrounds. *Please zoom in for detailed inspection.*

### 6.5 Hand-Specific Refl Generalization

Our hand-specific feedback reward mechanism demonstrates strong generalization to unseen gestures. During testing, we observed that it maintains a high degree of alignment with the accompanying text. As illustrated in Figure 9, when the character in the video says the word "twenty", the hand simultaneously performs a gesture corresponding to the number two, showcasing a remarkable level of semantic and temporal coherence. Notably, when we remove the proposed hand-specific reward mechanism, such gestures no longer emerge, indicating that our method significantly enhances the correspondence between hand motion and spoken content.



Figure 9: When the character says "twenty", the hand performs a two-finger gesture, demonstrating alignment between speech and hand gesture.

### 6.6 User Study Results

To evaluate the perceptual quality of the generated videos, six expert raters assessed 78 videos from two methods: InfinityHuman and Omnihuman (Lin et al. 2025). The evaluation covered overall video quality (high-standard and non-high-standard), compliance (e.g., stutter, clarity, commonsense), facial naturalness (hands, mouth, eyes), background distortion, and visual consistency (color, stability). Ratings were categorized as Excellent, Qualified, or Unqualified. The summarized results are presented in Table 5.

Overall, our method shows clear advantages in hand naturalness and image stability, with low failure rates of 2.6% and 1.3%, respectively, compared to significantly higher failure rates for Omnihuman. Besides, our method achieves a more

Category	Ours	Omnihuman
Total Videos	78 (100%)	78 (100%)
High-Standard Qualified	13 (16.7%)	0 (0.0%)
High-Standard Unqualified	65 (83.3%)	78 (100%)
Non-High-Standard Qualified	18 (23.1%)	0 (0.0%)
Non-High-Standard Unqualified	60 (76.9%)	78 (100%)
Video Compliance Qualified	78 (100%)	78 (100%)
Video Clarity Qualified	78 (100%)	77 (98.7%)
Hand Naturalness Unqualified	2 (2.6%)	41 (52.6%)
Mouth Naturalness (Excellent)	9 (11.5%)	7 (9.0%)
Background Distortion Unqualified	4 (5.1%)	18 (23.1%)
Image Stability Unqualified	1 (1.3%)	64 (82.1%)

Table 5: User study results: counts and percentages (%) of rated videos.

balanced overall quality and background consistency, highlighting its strengths in producing stable and natural outputs.

### 6.7 Long-Form Video Stability

To explore the stability of our model on long-form video generation, we segment each output into consecutive 10-second clips and compute cumulative metrics over time (i.e., 10s, 20s, 30s, etc.). This progressive evaluation enables us to analyze how performance evolves as video duration increases.

As shown in Table 6, our model maintains stable performance throughout extended video lengths. Specifically, key metrics such as FID, FVD, FSIM, and Sync show minimal degradation, indicating strong temporal consistency and robustness. In contrast, baseline models tend to suffer from more noticeable quality drops as duration increases.

Duration	FID ↓	FVD ↓	FSIM ↑	HKC ↑	Sync-C ↑
10s	36.83	1015.36	0.8357	0.9224	7.23
20s	37.07	1156.05	0.8323	0.9062	7.36
30s	35.02	1315.40	0.8266	0.8991	7.62
40s	35.92	1260.71	0.8154	0.9007	7.81
50s	35.50	945.84	0.8057	0.9059	7.46

Table 6: Cumulative evaluation on long-form video generation over increasing durations.

### 6.8 Societal Impacts

Our method enables the generation of high-fidelity talking head videos with synchronized hand gestures, which can benefit applications such as digital avatars, virtual presenters, and language learning tools. However, the ability to synthesize realistic human figures also poses potential risks. Inappropriate or malicious use of such technology—such as creating misleading or non-consensual content—could have negative societal consequences. To mitigate misuse, we advocate for strong watermarking, provenance tracking, and ethical deployment practices. Moreover, datasets used for training should be carefully curated to avoid reinforcing harmful biases or stereotypes. Future work should continue to emphasize fairness, transparency, and responsible AI development.

### 6.9 More Demo Cases

To further demonstrate the robustness and generality of our method, we provide several additional qualitative results across diverse scenarios.



Figure 10: Additional qualitative results showcasing the robustness and generality of our method across diverse scenarios.